Linear and nonlinear optical properties of a quadrupolar carbo-benzene and its benzenic parent: The carbo-merization effect

Rodrigo Barba-Barba, Marwa Chammam, Gabriel Ramos-Ortiz, Dymytrii Listunov, Jayaramakrishnan Velusamy, Mario Rodriguez, Ramon Carriles, Carlos Silva, Carine Guyard-Duhayon, Brice Kauffmann, et al.

Version of Record: https://www.sciencedirect.com/science/article/pii/S0143720821000012
Manuscript_acc6e0cf91df2e81cda220fb14e4ef45

Linear and nonlinear optical properties of a quadrupolar *carbo*-benzene and its benzenic parent: the *carbo*-merization effect

Rodrigo M. Barba-Barba[1,♣], Marwa Chammam[2,♣], Gabriel Ramos-Ortiz[1,3*], Dymytrii Listunov[2], Jayaramakrishnan Velusamy[1], Mario Rodriguez[1], Ramon Carriles[1], Carlos Silva[3,4], Carine Duhayon[2], Brice Kauffmann,[5] Valérie Maraval[2,*], Remi Chauvin[2,*]

[1] *Centro de Investigaciones en Óptica A.C., Apdo. Postal 1-948, 37000 Leon, Gto., Mexico*

[2] *LCC-CNRS, Université de Toulouse, CNRS, UPS, Toulouse, France*

[3] *School of Chemistry and Biochemistry, Georgia Institute of Technology, 901 Atlantic Drive NW, Atlanta, GA 30332, USA*

[4] *School of Physics, Georgia Institute of Technology,837 State Street, Atlanta, GA 30332, USA*

[5] *Université de Bordeaux, CNRS, INSERM, UMS3033/US001, Institut Européen de Chimie Biologie, 33607 Pessac, France*

Abstract: Herein, the optical properties of thiophene-functionalized quadrupolar *carbo*-benzenes and a benzenic parent, of generic structure Th-C≡C–[core]–C≡C–Th, Th = R_2C_4HS, are comparatively investigated. Beyond the previously unknown dioctylthiophenylethynylbenzene (core = *p*-C_6H_4, R = *n*Oct), two bis-dialkylthiophenylethynyl-*carbo*-benzenes (core = $C_{18}Ph_4$, R = *n*Oct, *n*Bu) are envisaged for the unique "*carbo*-aromatic" character of the C_{18} macrocycle. The three targets were synthesized from the corresponding ethynylthiophenes in 47, 20 and 10 % yield, respectively, then characterized by classical methods such as NMR spectroscopy, and X-ray crystallography for one of the *carbo*-benzenes. Regarding linear and nonlinear optical properties, our results show that the *carbo*-merization induces a significant shift to lower energies of the one-photon electronic excitations accompanied by an 8-fold increase of the molar extinction coefficient compared to the parent molecule**.** Intriguingly, these excitations lead to a broad band of photoluminescence comprising decay transitions of the

type $S_1 \rightarrow S_0$ but also of the type $S_2 \rightarrow S_0$. This phenomenon of emission from higher excited states, which is contrary to Kasha's rule, is assigned to - or revealed by - a reduction of the internal conversion efficiency between S_2 and S_1. Two-photon induced transitions are also enhanced, the two-photon absorption cross-section (σ_{2PA}) being in average five times larger for the *carbo*-benzenes than for their benzene parent in the wavelength range 650 – 950 nm, with a maximum of σ_{2PA} = 1430 GM (1 GM = 10^{-50} cm^4 s/photon). Beyond a moderate nonlinearity, this comparative study provides quantitative insights about the way *carbo*-merization or insertion of a π-conjugated macrocycle between chromophoric functions (here thiophene rings) can tune optical properties of organic molecules. The optical properties of the bis-dialkylthiophenylethynyl-*carbo*-benzenes are also discussed in regard of recent reports on organic chromophores based on other types of π-conjugated macrocyclic cores.

Keywords: *carbo*-benzenes, macrocycles, two-photon absorption, π-conjugation

•These authors contributed equally to this work

*Corresponding authors: **garamoso@cio.mx** (G.R-O); **valerie.maraval@lcc-toulouse.fr** (V.M); **chauvin@lcc-toulouse.fr** (R.C.)

1.- Introduction

During the last three decades, π-conjugated organic molecules and polymers have emerged as functional materials for diverse applications in the fields of optoelectronics and photonics [1]. Typically, the optical and electronic properties of these materials are tailored by designing molecular architectures with effective π-conjugated backbones, appropriate donor (D) and acceptor (A) electroactive substituents, and auxiliary functions. Classically,

the π-conjugation in molecules and polymers is brought by combination of unsaturated linear chains and/or small carbo- or hetero-cycles. Recently, a special type of π-conjugated backbone based on shape-persistent macrocyclic architectures have gained significant attention for two-photon absorption (2PA) or other nonlinear optical effects [2], optoelectronics [3], near-infrared luminescence [4], sensing of anions [5], photodynamic therapy [6], redox- or photo-responsive switches [7] and liquid crystallinity [8]. In such compounds, the number of π-electrons varies with the size of the macrocycle and in some cases intriguing electronic and optical properties are achieved even without the use of electroactive substituents [9]. Over the years, various π-conjugated macrocyclic architectures have been investigated, including macrocyclic annulenes [10], cyclic oligophenylenes and belt-shaped paraphenylenes [11], macrocyclic oligophenylene-ethynylenes [12], porphyrins and expanded porphyrins [13], and cyclic oligothiophenes [14]. More recently, novel macrocyclic architectures exhibiting aggregation-induced emission (AIE) properties have been designed [15]. Oligofuran-based macrocycles [16], polyradicaloids [17], hexagonal ring *carbo*-mers of benzene [18] and many others have been also considered.

The term *carbo*-mer designates "carbon enriched" molecules formally generated by systematic insertion of C_2 units into each (or a selected part) of the covalent bonds of a representative Lewis structure of any parent molecule [19]. At the Lewis-Gillespie level of representation, the *carbo*-merization process preserves the topology, symmetry, shape and π-electronic resonance of the parent molecule, while its bonding size is approximately expanded by a factor of three. Ring *carbo*-mers of benzene, simply called "*carbo*-benzenes", constitute the most exemplified series of *carbo*-mers [20], and have been

studied both theoretically, in particular for their aromaticity [21], and experimentally, *e. g.* for redox [18, 22], conductive [23], and mesogenic properties [24]. It was also demonstrated that *carbo*-benzenes exhibit unique chromophoric [18, 25] and nonlinear optical properties. In particular, the two-photon absorption (2PA) by the quadrupolar representatives (*p*-difluorenyl)tetraphenyl-*carbo*-benzene **1a** and (*p*-difluorenylethynyl)tetraphenyl-*carbo*-benzene **1b** (Figure 1) was recently evaluated, with a 2PA cross-section σ_{2PA} = 656 GM at 800 nm for **1b** [26]. This first attempt to assess the optical response of *carbo*-benzenes at infrared wavelengths showed their relevance as nonlinear materials. In this context, the understanding of the structure-optical properties relationships in *carbo*-mer series is still limited and awaits further investigation.

In this work, the effects of *carbo*-merization are evaluated through the comparison of the optical properties of the quadrupolar *carbo*-benzenes **2a,b** with those of the benzenic parent molecule **2P**, in which the central C_{18} macrocycle is replaced by a C_6 benzene ring (Figure 1). In these molecules, the thiophenyl substituents, largely used in the design of 2PA chromophores, behave as electronic donors that are anchored to the C_{18} macrocycle through an acetylenic linker. Dialkylthiophenylethynyl substituents were selected for two reasons: i) two alkyl chains are attached to the thiophene ring with the view of enhancing the solubility of the targeted *carbo*-benzenes **2a,b** to allow sufficiently high concentrations for the measurement of σ_{2PA} by the Z-scan technique (*ca* 10^{-3} - 10^{-2} mol.L^{-1}), and ii) the ethynyl linkers serve to both facilitate the synthesis key step, and increase the length of the π-conjugated system, thus *a priori* favoring high 2PA efficiency, as previously evidenced by the comparison between **1a** and **1b** (Figure 1). The linear photophysical properties (UV-vis

absorption, emission, excitation) and nonlinear optical properties (2PA) of the core-*carbo*-mers **2a** and **2P** are here reported in detail.

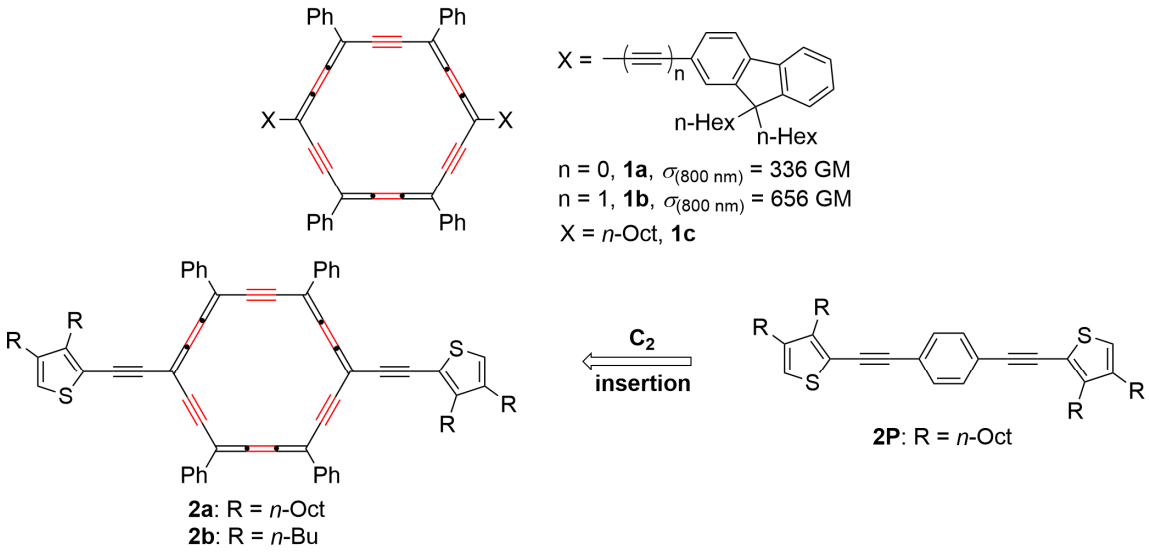

Figure 1. Quadrupolar *carbo*-benzenes **1a** and **1b** previously studied [26] for their 2PA properties (*top*); bis-thiophenylethynyl-*carbo*-benzenes **2a**,**b** and parent molecule **2P** considered in this work (*bottom*).

2. Results and discussion

2.1 Synthesis

The synthesis of the bis-dialkylthiophenylethynyl-*carbo*-benzenes **2a,b** required the preparation of known key precursors, namely the [6]pericyclynedione **3** [27], a classical intermediate in the synthesis of most quadrupolar *carbo*-benzenes [20], and the dialkylthiophenylacetylenes **4a,b**.

Though a synthesis of **4b** was previously published [28], **4a** and **4b** were not prepared following exactly the reported methodology. First, the described nickel-catalyzed Kumada coupling of commercial 3,4-dibromothiophene with octyl- or butyl-magnesium bromide led

to mixtures of dialkylthiophenes **5a,b** and monoalkylthiophenes **5a',b'** and in a 95:5 ratio (Scheme 1). In both cases, the separation of the two products by silica gel column chromatography appeared problematic because of their similar low polarity. The direct formylation of the mixtures **5a,b** and **5a',b'** leading to inseparable mixtures of aldehydes **6a,b** and **6a',b'**, the preparation of more polar intermediates was envisioned with the view to facilitating removal of the monoalkyl-thiophene contaminants. The mixtures of **5a,b** and **5a',b'** were thus treated with one equivalent of *n*-butyllithium, followed by addition of paraformaldehyde, to give mixtures of the alcohols **7a,b** and **7a',b'** which could then be separated by silica gel column chromatography. The pure alcohols **7a** and **7b**, isolated with 83 % and 95 % yield, respectively, were then oxidized by treatment with MnO_2 to give the corresponding aldehydes **6a** and **6b** almost quantitatively. Finally, the aldehydes were converted to the terminal alkynes **4a** and **4b** by a Corey-Fuchs reaction, in two steps *via* the dibrominated intermediates **8a,b** [29]**.**

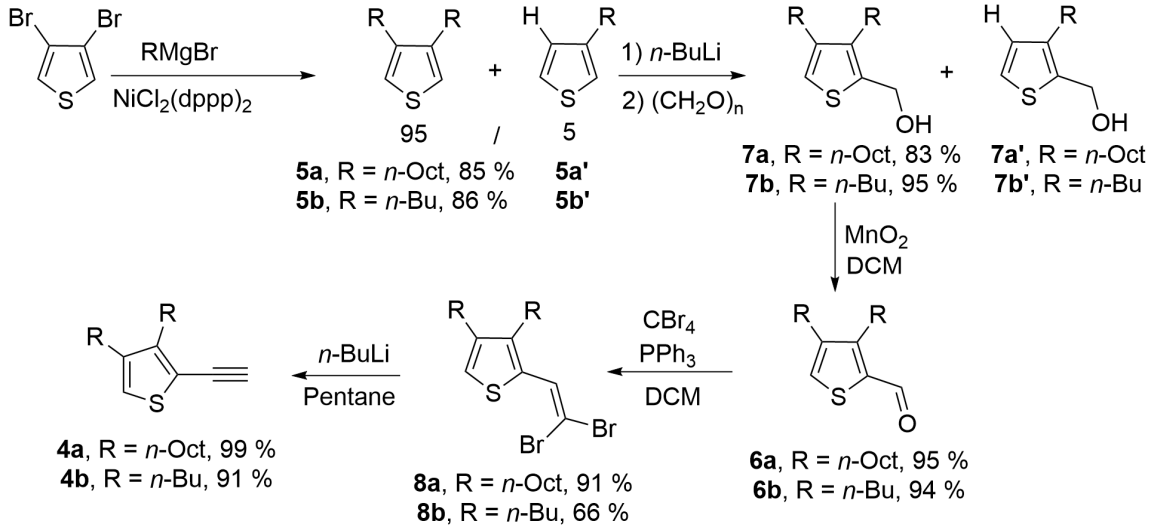

Scheme 1. Synthesis of the dialkylthiophenylacetylenes **4a,b**.

The *carbo*-benzenes **2a,b** were then prepared from **3** and **4a,b** by using the classical two-step process developed for the synthesis of other quadrupolar *carbo*-benzenes [20]. First, two equivalents of the lithium dialkylthiophenylacetylide of **4a** or **4b**, deprotonated with *n*-butyllithium, were added to the diketone **3**, leading to the pericyclynediols **9a,b** bearing the two thiophenylethynyl substituents. The last reductive aromatization step was performed with $SnCl_2$ alone to avoid the reduction and hydrochlorination of the exocyclic triple bonds, affording the *carbo*-benzenes **2a** and **2b** in 35 % and 20 % yield respectively (Scheme 2). In the presence of $SnCl_2$ and HCl, an inseparable mixture of chromophoric products was formed from **9a**, among which **2a'** could be identified by X-ray diffraction analysis (see SI, Figure S1). Such a hydrochlorination side-reaction was previously observed for [6]pericyclynediols bearing indolylethynyl donor groups, and its occurrence here with donor thiophenylethynyl groups is thus consistent [25c]. The unexpected reduction of the other triple bond to a *trans*-substituted double bond can be compared to a previously reported $SnCl_2$-mediated reduction of a *sp*C-*sp*C bond of a *carbo*-meric C_{18} ring to a *trans*-CH=CH bond [18].

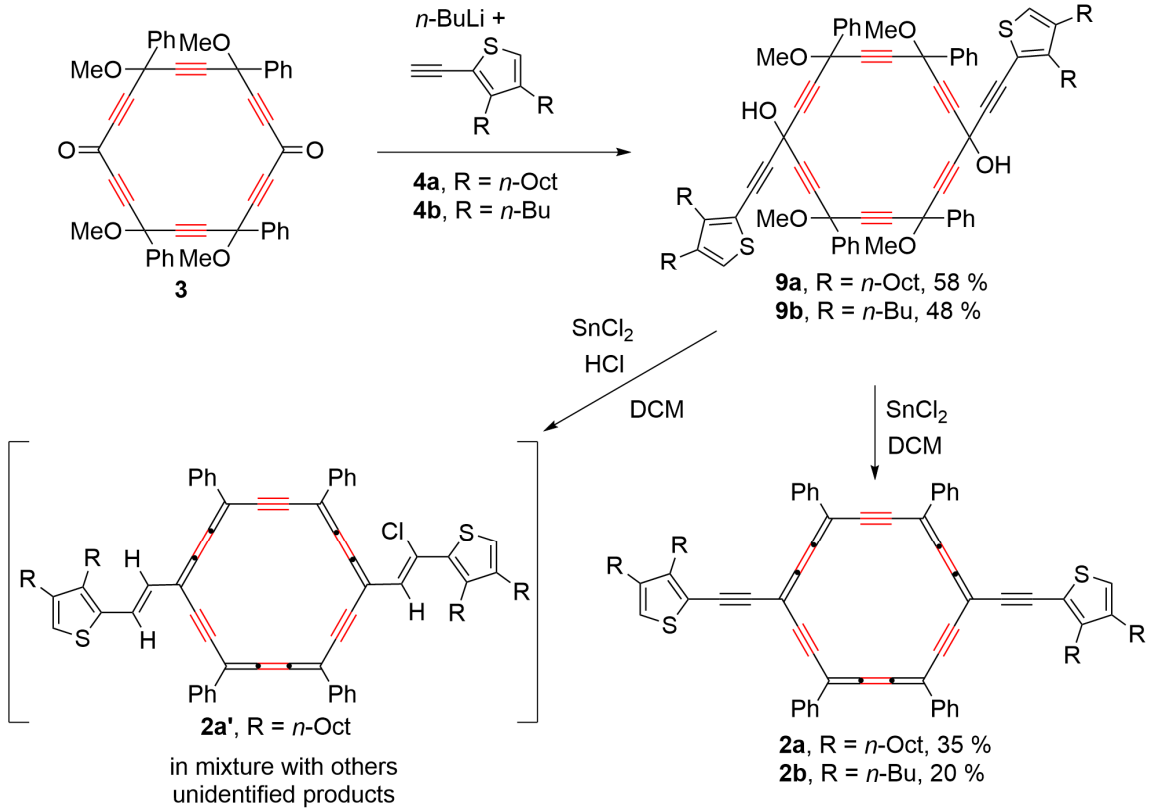

Scheme 2. Two-step synthesis of the *carbo*-benzenes **2a,b** from the known [6]pericyclynedione **3**.

The *carbo*-chromophores **2a,b** were isolated as violet solids, soluble in most of the conventional organic solvents while giving intense violet solutions. **2a** was characterized by NMR and UV-vis spectroscopy, and by mass spectrometry. Its structure was also determined by X-ray diffraction analysis of a single crystal deposited upon slow evaporation of a dichloromethane solution at room temperature (Figure 2 and Section 2.2) [30].

The parent molecule **2P** was prepared by a Sonogashira coupling of two equivalents of **4a** with diiodobenzene, and isolated with 47 % yield (Scheme 3).

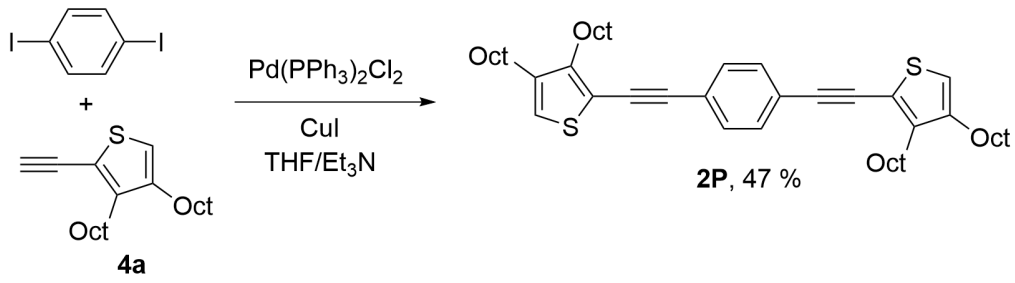

Scheme 3. Synthesis of the parent molecule **2P** of **2a**

2.2 *X-ray crystallography*

In the X-ray crystal structure of **2a** [30], the macrocycle is quasi planar, the maximum deviation from planarity being of 0.02 Å, with almost coplanar phenyl substituents (maximal torsion angle of 12.9°). The shape of the C_{18} ring is however quite distorted from a regular hexagon, the three $sp^2C\ldots sp^2C$ diagonal distances varying from 7.69 to 7.87 and 8.33 Å, while the internal bond angles vary from 116.9 to 121.8°, with two concave PhC···C≡C···C(C_2Th) edges.

In the crystal packing, the molecules of **2a** are shifted one from the other, but the mean planes of two successive macrocycles are parallel, albeit without normal overlapping between them. The distance between the mean planes of two successive molecules is of 3.26 Å. As one of the octyl groups is bent, some H atoms of the chain point towards the center of the closest *carbo*-benzene ring, the shortest distance measured between the centroid of the C_{18} ring and a H atom of the octyl chain being of 2.21 Å.

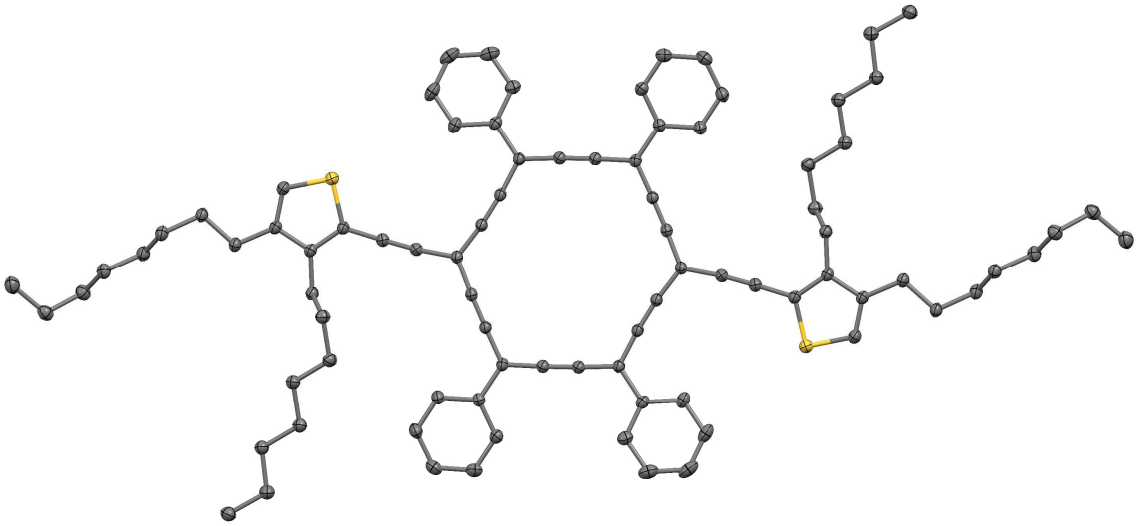

Figure 2. Molecular view of the X-ray crystal structure of **2a** (H atoms were omitted for clarity). See note [30], CCDC 2027203.

2.3 Electrochemistry

The electrochemical properties of the *carbo*-benzene **2b** were investigated by square-wave (SWV) and cyclic voltammetry (CV; Table 1). Four reduction and three oxidation waves were observed by SWV, the two first reductions at – 0.62 and – 1.02 V/SCE being reversible.

The first reduction is observed at a quite low potential (in absolute value), which is consistent with the extended π-conjugated system of **2b** *a priori* associated with a low LUMO level, and similar to the corresponding potential previously reported for **1b** (see Figure 1) [26].

The first oxidation, observed at 1.13 V/SCE, is a non-reversible process, as observed for **1b**, which is first oxidized irreversibly at 1.17 V/SCE.

Table 1. SWV and CV data for the *carbo*-benzene **2b.**

Reduction			Oxidation
$E_{1/2}$[a,b] (ΔE_p)	RI_p[c]	E_p^{red}[d]	E_p^{ox}[d]
- 0.62 (69)	0.99	- 1.52	1.13
- 1.02 (59)	0.76	- 1.74	1.75
			1.89

[a] Measurements performed at room temperature in DCM; supporting electrolyte: [nBu$_4$N][PF$_6$] (0.1 M); working electrode: Pt; reference electrode: saturated calomel electrode (SCE; 0.242 V *versus* the hydrogen electrode); scan rate: 0.2 V s^{-1}, unless otherwise noted. [b] Half-wave potential, $E_{1/2} = (E_p^{red} + E_p^{ox})/2$, in V/SCE. [c] Peak current ratio $RI_p = | I_p^{ox}/I_p^{red} |$. [d] E_p values measured from CV in V/SCE.

2.4 Optical properties

2.4.1 Linear optical properties

Effects of *carbo*-merization on optical properties can be evaluated by comparing the photoinduced electronic transitions of **2P** and **2a** (Figure 3). While **2P** exhibits an ordinary absorption band with a peak at 350 nm assigned to a $\pi \rightarrow \pi^*$ transition, **2a** presents the characteristic features of *carbo*-benzenes [18], with a sharp and intense band, in this case at 495 nm (for the simplicity of discussion this main band is denoted as **M** in Figure 3), a shoulder at 542 nm, and a secondary band with a peak at 608 nm (denoted as **S** band). The effect of dioctylthiophenylethynyl substitution at the *para* positions of the C_{18} macrocycle (C1 and C10 positions in **2a**) is clearly distinguishable by comparison with the absorption spectrum of the previously reported *para*-dialkyl-substituted analogue **1c** (Supplementary Information, Figure S2) with a much shorter π-conjugation extent [31]. The overall effect of substitution of the *carbo*-benzene ring with thiophenylethynyl units produces a bathochromic shift of *ca* 50 nm of both **M** and **S** bands as compared to **1c** accompanied by a moderate spectral broadening of the **M** band and vanishing of minor peaks between the **M** and **S** bands. The peak of maximum absorption for **2a** is practically at the same wavelength (495 nm) as the one observed for the fluorenylethynyl-substituted *carbo*-benzene **1b** [26] but with a *ca* 30% reduction of the molar extinction coefficient ε. Nevertheless, ε increases

from 2.8 $\times 10^4$ M^{-1} cm^{-1} in **2P** to 2.25 $\times 10^5$ M^{-1} cm^{-1} in **2a** due to the expansion of the π-conjugation. For organic molecules in general, the magnitude of ε is a signature of their polarizability at optical frequencies, which correlates with the degree of π-conjugation within the backbone and with substituents. For reference, Table 2 presents the optical properties and the molecular structure of some representative π-conjugated macrocycles. In these examples the number of π-electrons (m) in a conjugated circuit inscribed in the corresponding macrocycle varies from 18 to 180, producing molar extinction coefficients in the range 0.2 – 6.39 $\times 10^5$ M^{-1} cm^{-1}. In spite of a relatively low out-of-plane π_z-electron count m = 18 (unconjugated with the 12 in-plane π_{xy} electrons of the 6 *sp*C-*sp*C bonds), the ε values of *carbo*-benzenes are thus among the largest. According to the parity of m/2, the macrocycles of Table 2 can be qualitatively identified as aromatic *vs* antiaromatic using the well-known $m = 4n + 2$ *vs* $4n$ Hückel rule.

Table 2. Comparative properties for various π-conjugated macrocycles. The molecular structure of each of these macrocycles is presented in Table S1.

π-conjugated macrocycle	λ_{abs} **(nm)**	λ_{em} **(nm)**	$\varepsilon \times 10^5$ **(M^{-1} cm^{-1})**	***Conjugated π-electron count m and Hückel aromatic character*[a]**	σ_{2PA} **(GM)** σ_{2PA}/m **π-e** σ_{2PA}**/MW**	$\lambda_{max(TPA)}$ **(nm)**	**Ref.**
Thienylene-phenanthrylene	385	495	1.51	56 *antiaromatic*	-	-	32
Tetraphenylethylene based	330	520	-	*non-aromatic*	-	-	15
Oligofuran based	401	530	1.5	32 *antiaromatic*	-	-	16
BODIPY-phenylacetylene	364	527	0.26	32 *antiaromatic*	-	-	33
Phenanthrylene-ethynylidene	462	437	-	*non-aromatic*	-	-	34
Expanded 1,3-Dithiolane[5]radialene	403	.	1.2	*non-aromatic*	-	-	35
Triphenylamine phenylacetylene	380	430	-	*non-aromatic*	1 300 19.7 0.81	650	36
Triangle-shaped annulene	332	389	-	18 *aromatic*	11.5 0.64 0.031	372	37
Triangular –[D–π–A]$_3$–	375	469	2.0	66	2 800	750	38

				aromatic	42.42 0.85		
Phenylacetylene-based macrocycle	413	486	1.1	*non-aromatic*	125 4.2 0.069	820	39
Giant expanded oligothiophenes Thiophene[30]mer	480	559	6.18	180 *antiaromatic*	107 800 598 16.30	710	14, 40
Zinc(II) porphyrin	471	-	-	18 *aromatic*	3 520 195 2.66	1360	41
Hydrocarbon-substituted metal-free porphyrins	440	660	-	18 *aromatic*	42 600 2 366 38.33	800	42
Pentapyrrolic expanded porphyrin-isosmaragdyrin	712	716	-	22 *aromatic*	2 900 131.8 4.81	1280	43
Cyclo[8]pyrrole expanded porphyrin	427	1496	1.2	30 *aromatic*	3 030 101 3.12	1600	44
[26]Hexaphyrin expanded porphyrin	567	1036	4.2	26 *aromatic*	9 890 380 6.77	1200	44
Quadrupolar *carbo*-benzene **2a**	496		2.25	18 *aromatic*	1 430 83.3 2.12	650	This work

[a] Number *m* of conjugated π-electrons inscribed exclusively in the circuit of the corresponding macrocycle

It should be noted that characteristic features of the absorption spectra of *carbo*-benzenes, i.e., a sharp and intense **M** band followed by a secondary **S** band of weaker intensity, are not observed in other families of π-conjugated macrocycles (as those exemplified in Table 2) since they generally exhibit broad and structureless absorptions, except in the porphyrinoids whose spectra present the well-known Soret (B Band) and Q bands [13, 45]. The main band of the absorption spectra of substituted C_2-symmetrical *carbo*-benzenes was previously interpreted [26] as additive and subtractive combinations of excitations from the two highest occupied molecular orbitals (HOMO-1, HOMO) to the two lowest unoccupied molecular orbitals (LUMO, LUMO+1), as schematically shown in Figure 4. This approach invokes the Gouterman four-orbital model developed to explain the origin of the Soret and Q bands in the absorption spectra of porphyrins [45].

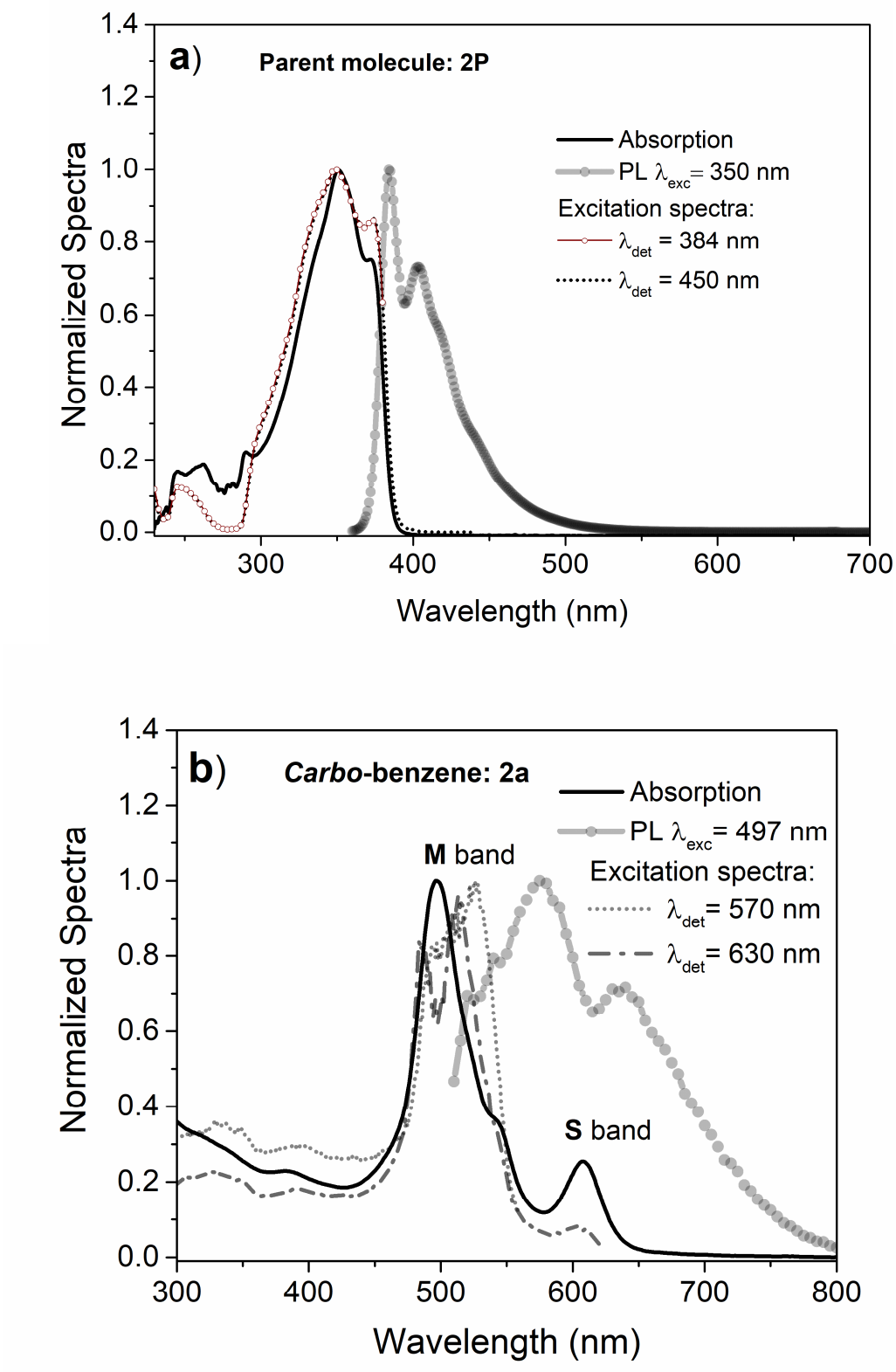

Figure 3. Absorption, PL (with excitation wavelength λ_{exc}) and excitation spectra (with detection of PL at the wavelength λ_{det}) obtained for a) **2P** and b) **2a** in THF solutions prepared at 8.43×10^{-5} M.

Figure 3 presents the photoluminescence (PL) spectra of **2P** and **2a** under excitation at their main absorptions, 350 and 497 nm, respectively. The PL spectrum of the parent molecule **2P** exhibits a band with a relatively small Stokes shift of 36 nm and noticeable vibronic structure. In the case of the *carbo*-benzene **2a**, the broad PL band is distorted due to absorption inner effects from the **S** band. Inner filter effects occurred inevitably in all the PL measurements of **2a** given its high ε and poor emission properties. Nevertheless, PL characterization of **2a** is worthwhile since it can provide information on the excited states that lead to radiative decays in *carbo*-benzenes. For example, radiative decays occur not only at longer wavelengths (lower energies) than the low-lying band **S**, but also at shorter wavelengths (higher energies). The matching between the PL excitation spectra and the absorption spectrum shown in Figure 3b clearly indicates that the electronic transitions corresponding to the **M** and **S** bands contribute to the PL emission. Furthermore, significant PL still occur at wavelengths with small shifts with respect to the excitation, suggesting small geometric changes between the excited and ground states. This is not surprising as we consider the planar and quite rigid monocyclic *carbo*-benzene ring, identified previously as both aromatic and flexible ("*carbo*-aromatic") [20c]. Small Stokes shifts are also observed in other planar conjugated systems such as the more rigid pentacyclic porphyrins and expanded porphyrins with residual flexibility [44]. Unexpectedly, the observation that PL can occur directly from the excitation of the **M** band is in contraposition with Kasha's rule [46] since it is assumed that such excitation leads to the quasi-degenerated exited state S_2 (see Figure 4 for the Jablonsky diagram proposed for **2a** in analogy with the Gouterman four-orbital model). PL from higher excited states ($S_2 \rightarrow S_0$) is a quite rare phenomenon that mainly occurs in small organic compounds [47] although it has also been reported in

macrocycles such as [18]annulene $C_{18}H_{18}$ [48], akin to *carbo*-benzene also identifiable as the most symmetric dodecadehydro-[18]annulene $C_{18}H_6$, BODYPI-based macrocycles [33], metalloporphyrins [49], and theoretically predicted in cyclo[n]thiophenes [50]. Anomalous emission had been also already observed for a dichromic *carbo*-cyclohexadiene [18] having a green PL band appearing between its blue and red absorption bands. However, this PL band was not explicitly identified as a radiative decay of the type $S_2 \rightarrow S_0$. The accepted interpretation for anomalous PL in organic molecules is that it can occur when the energy gap $\Delta E(S_2\text{-}\ S_1)$ is sufficiently large to reduce the Franck-Condon factor [51], the latter expressing the overlap integral of vibrational wavefunctions involved in the internal conversion (IC) process between S_2 and S_1, to a level where the rate of radiative $S_2 \rightarrow S_0$ transitions competes with the IC rate. Azulene, a polar hydrocarbon molecule, is a well-known prototype that exhibits efficient PL from S_2 due to a very large $\Delta E(S_2\text{-}\ S_1)$ ~ 10,000 cm^{-1} [47]. The *carbo*-chromophore **2a** also exhibits significant $\Delta E(S_2\text{-}\ S_1)$ ~ 3,673 cm^{-1}. This value is even larger for the *carbo*-cyclohexadiene reported in Ref[18], $\Delta E(S_2\text{-}\ S_1)$ ~ 6,272 cm^{-1}. This suggests that the fluorescence decay $S_2 \rightarrow S_0$ in **2a** could be assigned to the relatively wide separation between the **M** and **S** bands, which decreases, to some extent, the IC efficiency between S_2 and S_1, thus increasing the probability of bypassing S_1 during relaxations. It must be noted that the conformation of the macrocycle determines the density and shape of vibronic levels, and, in turn, the Franck–Condon factor. In consequence, the fluorescence in *carbo*-benzenes originates simultaneously from both the first and second excited states ($S_1 \rightarrow S_0$ and $S_2 \rightarrow S_0$) as depicted in Figure 4. All this characterization of the linear optical properties for 2P and 2a was obtained in dilute solutions such that self-assembly effects were discarded.

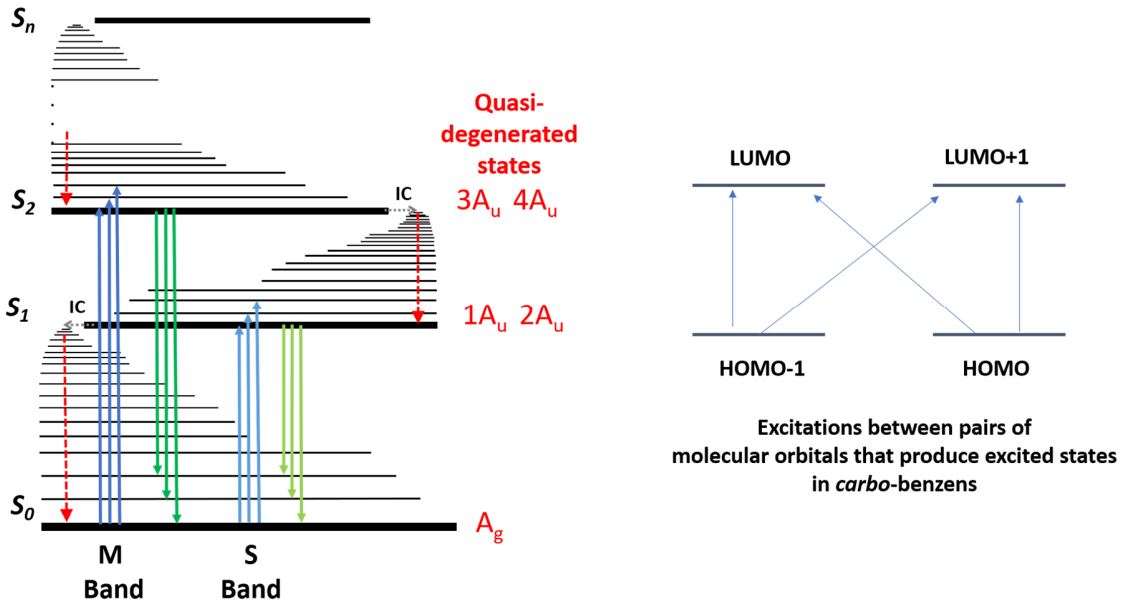

Figure 4. Jablonsky diagram (*left*) and Gouterman four-orbital model (*right*) for **2a**

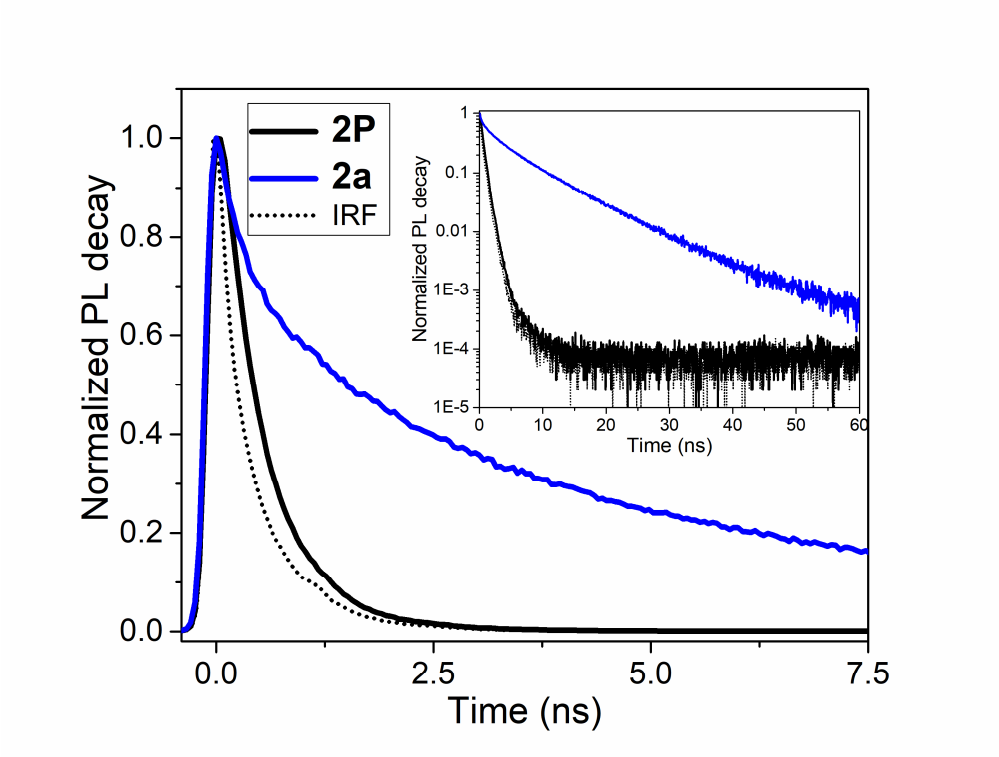

Figure 5. Lifetime measurements of **2a** (*blue line*) and **2P** (*black line*). As reference, the response function of the instrument (*dotted lines*) is presented. The emission lifetime of **2a** increases 5 times in comparison to the lifetime of **2P**. The lifetime of **2a** was monitored at 550 nm and **2P** at 414 nm. Inset: Plots in semilog scale.

As a consequence of *carbo*-merization, **2a** exhibited significantly longer fluorescence lifetime than its parent molecule **2P**. Figure 5 presents the PL decays of the two molecules using the technique of time-correlated single photon counting (TCSPC); in this figure, the dotted lines denote the instrument response, the solid lines the lifetimes of **2P** (black) and **2a** (blue). The average lifetime measured in **2a** was 5.04 ns, while the measurement for **2P** gave a significantly shorter value (1.02 ns), just barely different from the instrument response function. Although radiative decays from S_2 and S_1 should imply differentiated lifetimes, no wavelength dependence of the PL was observed, the resolution of the TCSPC technique probably being insufficient to allow their discrimination. Further investigation using techniques of higher temporal resolution will thus be necessary.

2.4.2 Nonlinear Optical Properties

Comparison of one- and two-photon excitations of **2P** and **2a** provides insight into the effects of *carbo*-merization on the energy level configuration and nonlinear polarizability. To measure σ_{2PA} in **2P,** the TPEF technique was used since that molecule fluoresces appreciably (quantum efficiency of 22%) and this technique is of higher sensitivity than Z-scan for molecules with small σ_{2PA} values. TPEF spectra of **2P** were recorded from 680 nm to 780 nm in a THF solution (8.43×10^{-5} M), as shown in Figure S3, and used to calculate the σ_{2PA} spectrum presented in Figure 6. In the case of **2a,** it was not possible to measure σ_{2PA} through the TPEF technique because of its very weak fluorescence. The σ_{2PA} spectrum of **2a** (THF solution at 8.43×10^{-2} M) was thus acquired from 650 nm to 950 nm through the Z-scan technique. To ensure a fair comparison of the nonlinearities obtained for the *carbo*-

meric and parent molecules through different techniques, the σ_{2PA} values of **2P** in solution (8.43×10^{-2} M in THF) were also determined by Z-scan at three different wavelengths (black dots in Figure 6), showing the agreement between the two techniques. In spite the high concentration of the solutions used in Z-scan experiments, self-assembly effects in 2P and 2a were not detected. For instance, light scattering, an affect that is typically produced in presence of self-assembled molecules, was not observed in the tested solutions. Of course, self-assembly could be present if the molecules are deposited in solid films, but such studies were beyond our present work. Larger nonlinearities are observed in **2a** with respect to **2P**, with a *ca* 7-fold increase in σ_{2PA} at the infrared (IR) range of wavelengths (which is, in fact, the region of interest for practical applications of the 2PA process). We can see that the onset of detectable nonlinear absorption in **2a** takes place at a significantly longer wavelength (950 nm, as shown in Figure S4) compared with **2P** (780 nm). Out of the IR range, the maximum values of σ_{2PA} were 506 GM for **2P** at 680 nm and 1430 GM for **2a** at 650 nm, with a tendency to increase at shorter wavelengths for both molecules. It is also illustrative to evaluate the enhancement of nonlinearities by comparison of the ratio between σ_{2PA} and the number m of π-electrons inscribed inclusively in the π-conjugated circuit. For instance, at IR wavelengths we have the relation σ_{2PA}/m (**2a**) ~ $2\times\sigma_{2PA}/m$ (**2P**). Thus, the overall linear and nonlinear characterization of **2a** shows that *carbo*-merization, though preserving the shape, symmetry and topology of a parent molecule, can induce enhancements of the polarizability (ε) and hyperpolarizability (σ_{2PA}) due to a wider π-conjugation extent and an improvement of the optical effects per π-conjugated electron. Table 2 presents σ_{2PA}/m values for a variety of macrocyclic chromophores. The *carbo*-benzene **2a** shows intermediate nonlinearities as compared to its counterparts. A similar

trend is observed when σ_{2PA} is normalized by the molecular weight. Note that in some series of macrocycles of increasing number *m*, an enhancement of nonlinearities is observed: giant oligothiophenes with *m* = 72 and 180 showed σ_{2PA}/m ~ 209 and ~ 598 GM, respectively [14]. In line with these observations, it would thus be of interest, at least at the theoretical level, to study the effect of enhancement or saturation of σ_{2PA} in *carbo*-mers of larger size than **2a**, for instance in *carbo*-benzenes of second generation exhibiting 30 cyclically π-conjugated electrons [20b].

The excited states accessible by two-photon transitions in substituted *carbo*-benzenes were examined. In Figure 6a, the total energy for a pair of infrared photons ($2\hbar\omega$) exciting **2a** is higher than the energy corresponding to the one-photon peak at the **M** band. This blue-shifting of the 2PA resonance with respect to one-photon resonance is expected in symmetric molecules like **2a** because one-photon and two-photon transitions are mutually exclusive according to Laporte's rule [51]. In the four-orbital model used to construct the excited states diagram of **2a**, the quasi-degenerate states $3A_u$ and $4A_u$ of the **M** band have an ungerade parity and are thus two-photon forbidden from the ground state of gerade parity (A_g). A strategy to enhance the nonlinearities at IR wavelengths of equivalent energies to the **M** band would thus be to lower the symmetry of *carbo*-benzenes by modifying the positions of the substituents of the C_{18} hexagonal core, strategy that was successfully applied with other macrocyclic molecules to bring 2PA states closer in energy to one-photon allowed states [52]. Of course, not only the symmetry of the molecule but also the nature and position of the substituents and π connectors play complementary roles that have to be globally taken into account in the design of new *carbo*-chromophore targets.

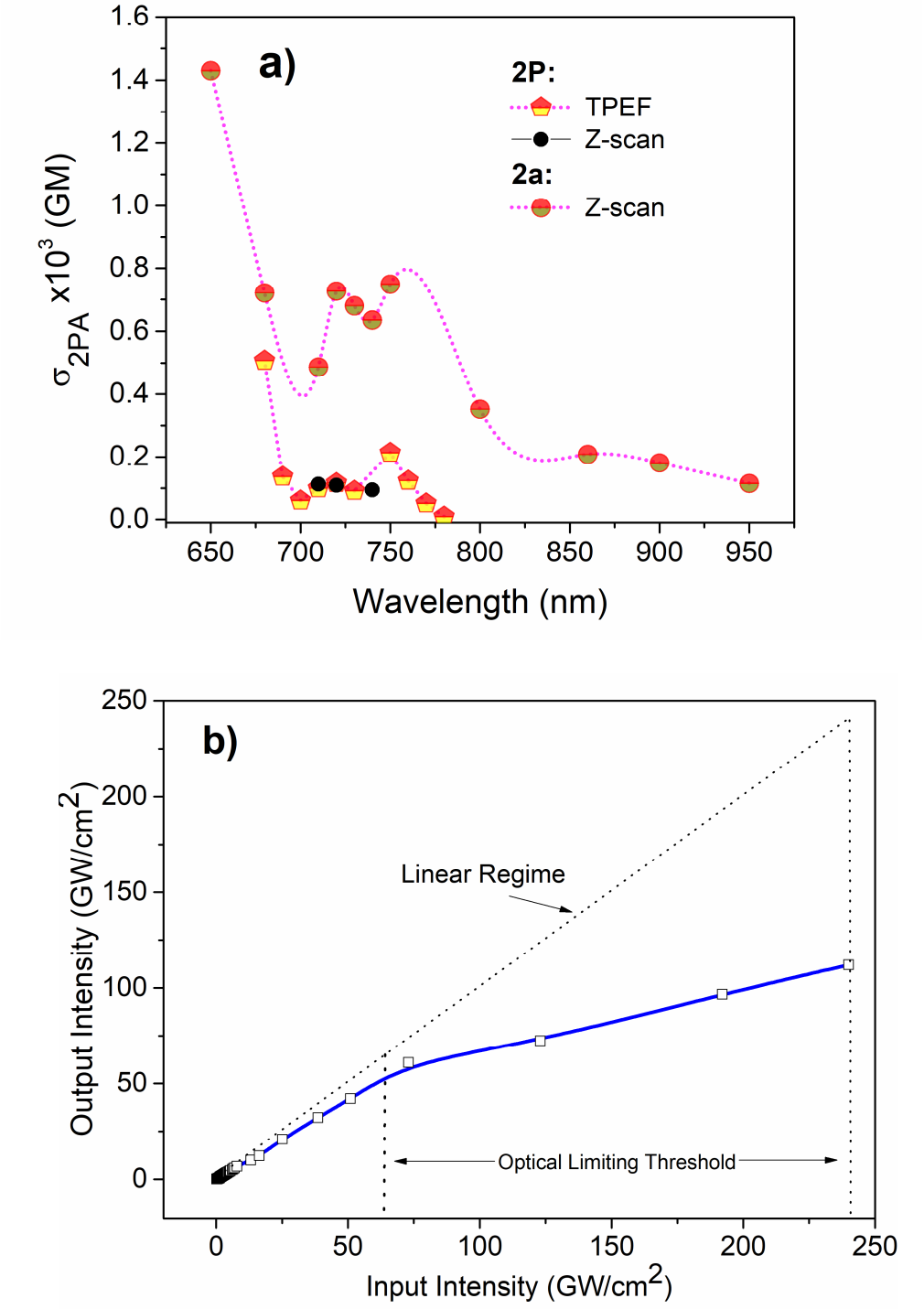

Figure 6. a) Spectra of the 2PA cross section for **2P** and **2a** measured in THF solution by TPEF and Z-scan techniques at the concentration of 8.43×10^{-5} and 8.43×10^{-2} M, respectively. 2PA cross sections were also measured for **2P** by Z-scan technique is a THF solution at 8.43×10^{-2} M; b) Optical limiting at 800 nm for **2a** emphasizing that, at the relatively low intensity of 20 GW/cm^2, its transmission diverges from a linear behavior.

Finally, the 2PA properties of the *carbo*-benzene **2a** allowed implementation of optical limiting, an application of utility for the protection of sensors, optical elements and human eyes. Measurements were performed at 800 nm with pulses of 80 fs and intensities ranging from 0.1 to 250 GW/cm^2. Even at energies as low as 20 GW/cm^2, **2a** begins to deviate from the linear regime getting to a maximum deviation at 60 GW/cm^2 (Figure 6b). For intensities as high as 250 GW/cm^2 no damage or degradation was detected in the sample, making **2a** appropriate for optical damage control [1c].

3.- Conclusions

To get insights into the underlying optical features that emerge in a given π-conjugated molecular topology when a C_6 benzene ring is replaced by a C_{18} aromatic macrocycle, the one- and two-photon-promoted electronic transitions were characterized in a quadrupolar *carbo*-benzene, namely **2a**, and compared with those of its parent molecule **2P**. In passing, but not less importantly, the synthesis and extensive characterization of the previously unknown *carbo*-benzene **2a**, homologue **2b**, and parent molecule **2P** are disclosed. In the linear regime, a notorious increment in the polarizability was observed, whereas, in the nonlinear regime, a higher 2PA activity per π-electron was determined. The presence of the hexagonal *carbo*-benzene ring in the conjugated backbone introduces anomalous PL due to simultaneous radiative decays $S_1 \rightarrow S_0$ and $S_2 \rightarrow S_0$. In view of these results, the C_{18} π-conjugated macrocycle can be considered as a versatile platform on which substituents can be attached at various positions in dipolar, quadrupolar or octupolar geometries, the two latter being relevant for potential applications involving 2PA as an initial process, or possibly for energy transfer from either the S_1 or S_2 excited states. Finally, the results also

suggest that lowering the symmetry of substituted *carbo*-benzenes, through replacement of some peripheral phenyl groups by other substituents, might allow tuning the peak of 2PA to longer wavelengths.

4.- Experimental section

4.1 *General*

THF, Et_2O, pentane and DCM were dried with a PureSolv-MD-5 Innovative Technology system for the purification of solvents. All other reagents were used as commercially available. In particular, solutions of *n*-BuLi were 1.6 or 2.5 M in hexane, solutions of EtMgBr were 3.0 M in THF, solution of *n*-OctMgBr were 2 M in Et_2O, solution of *n*-BuMgCl were 2.0 M in THF. All the reactions were carried out under an argon atmosphere by using Schlenk tube and vacuum line techniques. Column chromatography was carried out on silica gel (60 Å, C.C. 70-200 μm). Silica gel TLC plates (60F254, 0.25 mm) were observed under UV light and/or by treatment with a solution of phosphomolybdic acid (20 %) in ethanol. The following analytical instruments were used: ^{1}H and ^{13}C NMR spectroscopy: Avance 300, Avance 400 and Avance 400 HD spectrometers; MS: TSQ 7000 Thermo Electron and Voyager DE-ST Perseptive Biosystems spectrometers; UV/vis: Perkin-Elmer UV-vis Win-Lab Lambda 35; FT-IR: Perkin Elmer 1725.

NMR chemical shifts are given in ppm, with positive values to high frequency relative to the tetramethylsilane (TMS) reference. Coupling constants, *J*, are in Hz, UV-vis extinction molar coefficients, ε, are in L mol^{-1} cm^{-1}, wavelengths, λ, in nm.

4.2 Voltammetry

Voltammetric measurements were carried out with an Autolab PGSTAT100 potentiostat controlled by GPES 4.09 software. Experiments were performed at room temperature in a homemade, air-tight, three-electrode cell connected to a vacuum/argon line. The reference electrode consisted of a SCE separated from the solution by a bridge compartment. The counter electrode was a platinum wire of about 1 cm^2 apparent surface. The working electrode was a Pt microdisk (0.5 mm diameter). The supporting electrolyte, [nBu$_4$N][PF$_6$], was used as received (Fluka, 99 % electrochemical grade) and simply degassed under argon. The solution used in the electrochemical study was 10^{-3} M in *carbo*-benzene and 0.1 M in supporting electrolyte. Before each measurement, the solution is degassed by bubbling with argon, and the working electrode was polished by using a polishing machine (Presi P230). Typical instrumental parameters for recording SW voltammograms were: SW frequency, f = 20 Hz; amplitude, E_{sw} = 20 mV; scan increment dE = 0.5 mV.

4.3 Crystallography

Data collections were performed on a high flux microfocus Rigaku FRX rotating anode at the copper k$_\alpha$ wavelength equipped with a Dectris Pilatus 200K hybrid detector at 130 K. The structure was solved using Superflip [53a], and refined by full-matrix least-squares procedures on F using the programs of CRYSTALS [53b]. Atomic scattering factors were taken from the International tables for X-ray Crystallography [53c]. All non-hydrogen atoms were refined anisotropically. Hydrogen atoms were refined using a riding model. Absorption corrections were introduced using the program MULTISCAN.

4.4 Synthesis and characterization

- **2-(2-{10-[2-(3,4-dialkylthiophen-2-yl)ethynyl]-4,7,13,16-tetraphenylcyclooctadeca-1,2,3,7,8,9,13,14,15-nonaen-5,11,17-triyn-1-yl}ethynyl)-3,4-dialkylthiophene (2a, 2b)**

To the solution of **9a** or **9b** (0.025 mmol) in 20 mL of dry DCM at -78°C was added anhydrous $SnCl_2$ (20 eq.), and the resulting mixture was allowed warming to room temperature and stirred at this temperature for 3 h. Then the mixture was filtered through a pad of silica gel using DCM until complete elution of colored fractions. The resulting colored solutions were joined and concentrated under vacuum and the residue were washed with pentane to give **2a** or **2b** as a dark violet solid (**2a**: 35%, **2b**: 20%).

2a: **^{1}H NMR** (CD_2Cl_2, 400 MHz): δ 0.61 (t, J = 7.1 Hz, 6H), 0.94 (t, J = 6.6 Hz, 6H), 1.01 –1.13 (m, 8H), 1.17 – 1.29 (m, 4H), 1.32 –1.58 (m, 24H), 1.65 (quint, J = 7.2 Hz, 4H), 1.81 (quint, J = 7.6 Hz, 4H), 1.99 (quint, J = 8.7, Hz, 4H), 2.75 (t, J = 7.8 Hz, 4H), 3.28 (t, J = 7.7 Hz, 4H), 7.26 (s, 2H), 7.73 (t, J = 7.5 Hz, 4H), 7.96 (t, J = 7.8 Hz, 8H), 9.43 (d, J = 7.5 Hz, 8H).

^{13}C {^{1}H} NMR (CD_2Cl_2, 100 MHz): δ 14.1, 14.3, 22.9, 23.2, 29.3, 29.6, 29.7, 29.8, 30.0, 30.0, 30.1, 30.1, 30.4, 30.9, 32.1, 32.4, 85.1, 94.0, 97.6, 105.1, 114.0, 118.7, 119.4, 120.0, 124.8, 130.3, 130.3, 130.4, 139.4, 143.7, 150.2.

HRMS (MALDI-TOF/DCTB): *m/z* calcd for $C_{86}H_{90}S_2$ $[M^*]$+ 1186.6484, found: 1186.6416.

UV-Visible ($CHCl_3$): λ_{max}= 497 nm (ε = 225 000 L·mol^{-1}·cm^{-1}).

2b: **^{1}H NMR** ($CDCl_3$, 300 MHz): δ 1.06 – 1.13 (m, 12H), 1.57 (m, 4H), 1.72 – 2.01 (m, 12H), 2.75 (t, J = 7.8 Hz, 4H), 3.28 (t, J = 7.6 Hz, 4H), 7.22 (s, 2H), 7.75 (t, J = 7.3 Hz, 4H), 7.97 (t, J = 7.7 Hz, 8H), 8.46 (d, J = 7.3 Hz, 8H).

HRMS (MALDI-TOF/DCTB): *m/z* calcd for $C_{70}H_{58}S_2$ $[M^*]$+ 962.3943, found: 962.3980.

- **2-(2-{4-[2-(3,4-dioctylthiophen-2-yl)ethynyl]phenyl}ethynyl)-3,4-dioctylthiophene (2P)**

To a degassed solution of 1,4-diiodobenzene (48 mg, 0.143 mmol) and **4a** (100 mg, 0.301 mmol) in a mixture of dry THF/Et_3N (5 mL, 4/1) under an argon atmosphere were added copper(I) iodide (3 mg, 0.0143 mmol) and bis(triphenylphosphine)palladium(II) dichloride (5 mg, 0.00715 mmol). The mixture was heated in a sealed tube at 75°C for 12 h before cooling to room temperature and concentration under vacuum. The residue was purified by SiO_2 column chromatography (pentane : EtOAc = 10 : 1) to give **2P** as a waxy solid (49 mg, 47%).

^{1}H NMR ($CDCl_3$, 400 MHz): δ 0.84-0.95 (m, 12H), 1.22-1.47 (m, 40), 1.56-1.69 (m, 8H), 2.51 (t, J = 7.6 Hz, 4H), 2.71 (t, J = 7.6 Hz, 4H), 6.88 (s, 2H), 7.42-7.48 (s, 4H).

^{13}C {^{1}H} NMR ($CDCl_3$, 100 MHz): δ 14.1, 22.7, 28.3, 29.1, 29.3, 29.3, 29.4, 29.5, 29.5, 29.6, 29.8, 30.0, 31.9, 31.9, 85.2, 94.6, 118.3, 121.7, 123.0, 131.0, 142.2, 147.3.

HRMS (MALDI-TOF/DCTB): *m/z* calcd for $C_{50}H_{74}S_2$ $[M^*]^+$ 738.5232, found: 738.5288.

- **2-ethynyl-3,4-dialkylthiophene (4a,b)**

n-BuLi (1.2 eq.) was added at -78 ° C to a solution of dibromoolefin **8a** or **8b** (13 mmol,1 eq.) in pentane (300 mL). The temperature was increased up to *ca* -40 ° C and stirring was continued for 30 min. Then, the mixture was cooled again to -78 ° C and treated with a saturated aqueous solution of NH_4Cl. After extractions of the aqueous layer with diethyl ether, the combined organic layers were washed with brine, dried over $MgSO_4$ and evaporated under reduced pressure to give the expected product **4a** or **4b** as a yellow liquid (**4a**: 99%, **4b**: 91%).

4a: **^{1}H NMR** (400 MHz, $CDCl_3$) δ 0.90 – 0.93 (m, 6H), 1.29 – 1.41 (m, 24H), 1.55 – 1.63 (m, 4H), 2.51 (t, J = 8.0 Hz, 2H), 2.66 (t, J = 8.0 Hz, 2H), 3.43 (s, 1H), 6.84 (s, 1H).

^{13}C {^{1}H} NMR ($CDCl_3$, 100 MHz) δ 14.1, 22.7, 28.1, 29.0, 29.3, 29.3, 29.4, 29.5, 29.5, 29.6, 29.8, 30.0, 31.9, 31.9, 82.6, 117.3, 121.4, 141.9, 148.1

HRMS (DCI/CH_4): *m/z* calcd for $C_{22}H_{37}S$ $[M-H]^+$ 333.2616, found: 333.2603.

IR (cm^{-1}): ν = 3313, 2954, 2923, 2854, 2101, 1465, 1155, 875, 744, 655, 575.

4b: the obtained data were in accordance with those previously described [28].

• **3,4-dialkylthiophenes (5a, 5b)** were prepared following described procedures. Physical properties of the obtained products are in accordance with those previously reported [28, 54]

• 3,4-dialkyl-2-thiophenocarboxaldehyde (6a, 6b)

A solution of the alcohol **7a** or **7b** (1 eq., 15 mmol) in DCM (300 mL) was treated with MnO_2 (10 eq.) at 0°C. The mixture was stirred at 0°C for 10 min., then 1.5 h at room temperature, before being filtered through celite®. The solution was concentrated under vacuum to give the expected spectroscopically pure aldehydes **6a** or **6b** as a yellow oil (**6a**: 95%, **6b**: 94%)

6a: the obtained data were in accordance with those previously described [54].
6b: the obtained data were in accordance with those previously described [55].

• 2-Hydroxymethyl-3,4-dialkylthiophene (7a,7b)
n-BuLi (1.2 eq.) was added at 0 °C to a solution of the **6a, 6a'** or **6b, 6b'** mixture (1 eq., 16 mmol) in THF (50 mL). After 45 minutes of stirring, the mixture was brought to room temperature and a suspension of paraformaldehyde (1.8 eq.) in THF (10 mL) was added. The mixture was stirred for 3 h at room temperature, and poured into ice and water. Then, the pH was adjusted to 6 by addition of concentrated HCl. After extractions of the aqueous

layer with diethyl ether, the combined organic layers were washed with water, dried over $MgSO_4$ and evaporated under reduced pressure. After purification by silica gel chromatography (pentane : diethyl ether, 98 : 2), the alcohols **7a** or **7b** were obtained as a yellow liquid (**7a**: 83%, **7b**: 95%)

7a: t he obtained data were in accordance with those previously described [54].

7b: the obtained data were in accordance with those previously described [56].

• ((1,1-Dibromo) -2-ethene) -3,4-dialkylthiophene (8a,8b)

A solution of aldehyde **6a** or **6b** (1 eq., 15 mmol) in DCM (200 mL) was added at 0 °C to a mixture of PPh_3 (4 eq.) and CBr_4 (2 eq.) in DCM (50 mL). The resulting mixture was stirred for 5 min. before being concentrated to dryness. The residue was purified by silica gel chromatography (pentane : EtOAc 100 : 1) to give the expected product **8a** or **8b** as a yellowish liquid (**8a**: 91%, **8b**: 66%).

8a: **^{1}H NMR** (300 MHz, $CDCl_3$) δ 0.96 (t, J = 8.0 Hz, 6H), 1.34 – 1.40 (m, 22H), 1.64 – 1.70 (m, 2H), 2.53 – 2.60 (m, 4H), 7.04 (s, 1H), 7.68 (s, 1H).

^{13}C {^{1}H} NMR ($CDCl_3$) δ 14.2, 22.8, 27.4, 28.8, 29.3, 29.4, 29.4, 29.6, 29.7, 29.7, 29.8, 31.0, 32.0, 85.9, 121.7, 129.9, 131.9, 141.8, 143.2.
HRMS (DCI/CH_4): *m/z* calcd for $C_{22}H_{36}OSBr_2$ [M] 490.0904, found: 490.0904.

8b: **^{1}H NMR** (300 MHz, $CDCl_3$) δ 0.97 (m, 6H), 1.39 – 1.62 (m, 12H), 2.50 – 2.60 (m, 4H), 7.03 (s, 1H), 7.64 (s, 1H).

^{13}C {^{1}H} NMR (75 MHz, $CDCl_3$): δ 13.9, 14.0, 22.6, 22.7, 27.2, 28.4, 31.9, 33.1, 85.9, 121.7, 129.8, 131.8, 141.8, 143.2.
HRMS (DCI/CH_4): *m/z* calcd for $C_{14}H_{20}OSBr_2$ [M] 377.9639, found: 377.9652.

- **1,10-bis[2-(3,4-dialkylthiophen-2-yl)ethynyl]-4,7,13,16-tetramethoxy-4,7,13,16-tetraphenylcyclooctadeca-2,5,8,11,14,17-hexayne-1,10-diol (9a, 9b)**

To the solution of **4a** or **4b** (3 eq.) in dry THF (10 mL) at -78°C was added dropwise a *n*-BuLi solution (1.6 M in hexane, 2.5 eq.). Stirring was continued at -78°C for 30 min., then at room temperature for 1 h. After cooling to -78°C, a solution of **3** (0.15 mmol) in dry THF (2 mL) was added dropwise and the mixture was allowed warming slowly to room temperature overnight. The reaction was treated with a saturated aqueous solution of NH_4Cl and the aqueous layer was extracted with Et_2O. The combined organic layers were dried with $MgSO_4$, concentrated under vacuum and purified by SiO_2 column chromatography (pentane : EtOAc 10 : 1) leading to the diol **9a** or **9b** as a waxy solid (**9a**: 58%, **9b**: 48%).

9a: **^{1}H NMR** ($CDCl_3$, 300 MHz): δ 0.84 – 0.94 (m, 12H), 1.18 – 1.65 (m, 24H), 2.49 – 2.67 (8H), 2.93 – 3.21 (m, 2H), 3.41 – 3.68 (m, 12H), 6.92 (s, 2H), 7.28 – 7.42 (m, 12H), 7.74 – 7.82 (m, 8H).

^{13}C {^{1}H} NMR ($CDCl_3$, 100 MHz): δ 14.1, 22.7, 28.3, 28.9, 29.2, 29.4, 29.5, 29.7, 29.8, 30.0, 30.1, 31.9, 53.6, 54.9, 71.9, 78.3, 80.4, 84.4, 90.5, 116.1, 123.0, 126.5, 128.5, 129.1, 139.2, 142.2, 149.0

HRMS (MALDI-TOF/DCTB): *m/z* calcd for $C_{86}H_{90}S_2$ $[M]^+$ 1186.6484, found: 1186.6460.

9b: **^{1}H NMR** ($CDCl_3$, 300 MHz): δ 0.88 – 0.98 (m, 12H), 1.27 – 1.59 (m, 16H), 2.48 – 2.62 (m, 8H), 3.52 – 3.54 (m, 12H), 6.88 (s, 2H), 7.29 – 7.33 (m, 12H), 7.74 (m, 8H).

MS (MALDI-TOF/DCTB): *m/z* $[M\text{-}Na]^+$ 1143.7 $[M\text{-}K]^+$ 1159.7

4.5 Linear and nonlinear spectroscopic characterization

Spectra of linear absorption, emission, excitation, and lifetime of fluorescence were obtained with the use of a fluorometer (FS5, Edinburgh Instruments). Emission was also

obtained by pumping the sample with short optical pulses (100 kHz repetition rate) from an optical parametric amplifier (Orpheus, Light Conversion, Lithuania) pumped at 1030 nm by a mode-locked oscillator (Pharos—Model PH1-20-0200-02-10, Light Conversion, Lithuania). To minimize absorption inner effects, the excitation and recollection of emission was produced in the front face of a 1mm-thick cuvette containing a solution of the sample. The emission analyzed with an imaging spectrograph (Shamrock 193i, Andor Technology) and detected with a multichannel detector. The σ_{2PA} was obtained by Z-scan method with 80 fs (800 nm) laser pulses delivered by a Ti:Sa amplifier (Libra HE from Coherent) at 1 KHz. At the position Z = 0 the beam waist was 20 μm. THF solutions were tested at the concentration of 8.43×10^{-2} M in a 1 mm quartz cell. For wavelengths other than 800 nm in the range 650 to 950 nm, the Z-scan method was implemented with an optical parametric amplifier (TOPAs, from Light Conversion). The nonlinear coefficient β was calculated from the equation [57]:

$$T(z) = 1 - \frac{1}{2\sqrt{2}}\beta\frac{I_0 L_{eff}}{1+(Z/Z_0)^2} \quad (1)$$

Where I_0 is the peak intensity, L_{eff} is the effective length of the sample with $\mathbf{L_{eff}} = [\mathbf{1} - \mathbf{exp}(-\boldsymbol{\alpha_0}\mathbf{L})]/\boldsymbol{\alpha_0}$, where L is the sample thickness and $\boldsymbol{\alpha_0}$ the absorption coefficient, Z the sample position and $\mathbf{Z_0} = (\boldsymbol{\pi\omega_0^2}/\boldsymbol{\lambda})$ the Rayleigh range. To determine $\boldsymbol{\omega_0}$ the knife edge method was used. The Z-scan apparatus was calibrated with traces in the close aperture scheme using CS_2 as standard nonlinear refractive material with $\mathbf{n_2}= 2\times10^{-15}$ cm^2/W [58]. Finally, $\boldsymbol{\sigma_{2PA}} = \frac{\hbar\boldsymbol{\omega}}{\mathbf{N}}\boldsymbol{\beta}$, where $\hbar\omega$ is the photon energy and N the density of molecules in the solution.

Two- photon excited fluorescence (TPEF) was implemented with 140 fs pulses from a Ti:Sa oscillator (Chameleon ultra, from Coherent) in the range 680-1080 nm. THF

solutions were tested at a concentration of 8.43×10^{-5} M. Laser beam was focused in the frontal face of a 1 cm quartz cell with a 35 mm focal length lens. TPEF signal was detected in the perpendicular direction to the excitation with a hand-held spectrometer (Ocean optics, 2000+) and using a low pass filter to block the excitation. The $\boldsymbol{\sigma_{2PA}}$ value was obtained using the equation[59]:

$$\sigma_{TPA} = \sigma_R \frac{F_S C_R \Phi_R \eta_R}{F_R C_R \Phi_S \eta_S} \quad (2)$$

where, F is the integrated area of the emission, C is the molar concentration (mol. L^{-1}), $\boldsymbol{\Phi}$ is the fluorescence QY, and η is the refraction index of the solvent, the subscripts S and R denoting sample and reference, respectively. The Rodhamine 6G at a concentration of 1×10^{-5} M was used as reference for calibration.

4.6 Optical Limiting

For optical limiting measurements, the same laser source as the Z-scan experiments was used at 800 nm. The setup consisted in a laser beam hitting a 1mm quartz cell containing a solution of **2a** at a concentration of 8.43×10^{-2} M in THF.

Acknowledgements

The work has been performed within the framework of ECOS-NORD project (M16P02 and 291434) and the French Mexican International Laboratory LIA-LCMMC with financial support from CNRS (France) and CONACYT (Mexico). M. B.-B. thanks CONACYT for his PhD fellowship (565612). M. C. thanks the French Ministère de l'Enseignement Supérieur de la Recherche for her PhD scholarship. The authors thank the IDEX Emergence program 2014 (Carbo-device) for the post-doctoral grant of D. L. and for funding. The Centre National de la Recherche Scientifique (CNRS) is also acknowledged

for funding. The work at the Georgia Institute of Technology was supported by the National Science Foundation (DMR-1729737). This work has benefited from the X-ray facility of the Biophysical and Structural Chemistry platform at IECB, CNRS UMS3033, INSERM US001, Bordeaux University.

References

[1] a) Organic Electronics Materials and Devices, Ed. Shuichiro Ogawa, Springer 2015; b) Gu B, Zhao C, Baev A, Yong KT, Wen S, Prasad PN. Molecular nonlinear optics: recent advances and applications. Advances in Optics and Photonics 2016;8: 328-9; c) Nalwa HS, Nonlinear Optics of Organic Molecules and Polymers, Opt. Eng. (1997).
[2] a) Iyoda M, Yamakawa J, Rahman MJ. Conjugated Macrocycles: concepts and applications. Angew Chem Int Ed 2011;50:10522-53; b) Senge MO, Fazekas M, Notaras EGA, Blau WJ, Zawadzka M, Locos OB, Ni Mhuircheartaigh EM. Nonlinear optical properties of porphyrins. Adv Mater 2007;19:2737-74; c) Sajid H, Ayub K, Mahmood T. Exceptionally high NLO response and deep ultraviolet transparency of superalkali doped macrocyclic oligofuran rings. New J Chem 2020;44:2609-18; d) Liu Z, Lu T. Controllable photophysical and nonlinear properties in conformation isomerization of macrocyclic [32]octaphyrin(1.0.1.0.1.0.1.0) involving Hückel and Möbius topologies. J Phys Chem C 2020;124;845-53.
[3] a) Izumi S, Higginbotham HF, Nyga A, Stachelek P, Tohnai N, de Silva P, Data P, Takeda Y, Minakata S. Thermally activated delayed fluorescent donor-acceptor-donor-acceptor π-conjugated macrocycle for organic light-emitting diodes. J Am Chem Soc 2020;142:1482-91; b) Izumi T, Tian Y, Ikemoto K, Yoshii A, Koretsune T, Arita R, Kita H, Taka H, Sato S, Isobe H. Efficient blue electroluminescence from a single-layer organic device composed solely of hydrocarbons. Chem Asian J 2017;12:730 -3; c) Ball M, Zhang B, Zhong Y, Fowler B, Xiao S, Ng F, Steigerwald M, Nuckolls C. Conjugated macrocycles in organic electronics. Acc Chem Res 2019;52:1068-78.
[4] a) Yao Y, Hou CL, Yang ZS, Ran G, Kang L, Li C,Zhang W, Zhang J, Zhang JL. Unusual near infrared (NIR) fluorescent palladium(II) macrocyclic complexes containing M-C bonds with bioimaging capability. Chem Sci 2019;10:101708; b) Mallick A, Oh J, Kim D, Rath H. Aromatic fused [30] heteroannulenes with NIR absorption and NIR emission: synthesis, characterization, and excited-state dynamics. Chem Eur J 2016;22:8026-31.
[5] Gregolińska H, Majewski M, Chmielewski PJ, Gregoliński J, Chien A, Zhou J, Wu YL, Bae YJ, Wasielewski MR, Zimmerman PM, Stępien M. Fully conjugated [4]chrysaorene. Redox-coupled anion binding in a tetraradicaloid macrocycle. J Am Chem Soc 2018;140:14474-80.
[6] *Cancer Theranostics*, Eds. Edited by: Chen X and Wong S, Chapter 14, 229-254 (2014).
[7] a) Martynov AG, Safonova EA, Tsivadze AY. Functional molecular switches involving tetrapyrrolic macrocycles. Coord ChemRev 2019;387:325-47; b) Canarya JW. Redox-triggered chiroptical molecular switches. Chem Soc Rev2009;38:747-56.

[8] Kawano SI, Kato M, Soumiya S, Nakaya M, Onoe J, Tanaka K. Columnar liquid crystals from a giant macrocycle mesogen. Angew Chem Int Ed 2018;57:167-71.
[9] Wild UP, Griesser HJ, Tuan VD, Oth JFM. Fluorescence from the second excited singlet state of [18] annulenes. Chem Phys Lett 1976;41:4505.
[10] Spitler EL, Johnson II CA, Haley MM. Renaissance of annulene chemistry. Chem Rev 2006; 106:5344-86.
[11] a) Iyoda M. Copper-mediated aryl-aryl couplings for the construction of oligophenylenes and related heteroaromatics. Adv Synth Catal 2009;351:984-98 ; b) Pham ST, Ikemoto K, Suzuki KZ, Izumi T, Taka H, Kita H, Sato S, Isobe H, Mizukami S. Magneto-electroluminescence effects in the single-layer organic light-emitting devices with macrocyclic aromatic hydrocarbons. APL Materials 2018;6:026103; c) Wu D, Cheng W, Ban X, Xia J. Cycloparaphenylenes (CPPs): an overview of synthesis, properties, and potential applications. Asian J Org Chem 2018;7:21-81.
[12] a) Zhong Y, Wang Q, Yang Y, Lu Z, He L, Gong B. Hexakis(m-phenylene ethynylene) macrocycles with multiple H-bonding side chains and modified cavities: altered stacking strength and persistent tubular assembly. Org.Lett 2016;18:2094-97; b) Zhang W, Moore JS. Shape-persistent macrocycles: structures and synthetic approaches from arylene and ethynylene building blocks. Angew Chem Int Ed 2006;45:4416-39; c) Zhao D, Moore JS. Shape-persistent arylene ethynylene macrocycles: synthesis and supramolecular chemistry. Chem Commun 2003;807-18.
[13] a) Saito S, Osuka A. Expanded porphyrins: intriguing structures, electronic properties, and reactivities. Angew Chem Int Ed 2011;50:4342-73; b) Porphyrins and metalloporphyrins, Falk J. E., Elservier (1975); c) Nemykin VN, Hadt RG. Interpretation of the UV-vis spectra of the meso(ferrocenyl)-containing porphyrins using a TDDFT approach: is Gouterman's classic four-orbital model still playing? J Phys Chem A 2010;114:12062-6.
[14] Iyoda M, Shimizu H. Multifunctional π-expanded oligothiophene macrocycles. Chem Soc Rev 2015;44:6411-24.
[15] Liu Y, Lin FX, Feng Y, Liu X, Wang L, Yu ZQ, Tang BZ. Shape-persistent π-conjugated macrocycles with aggregation-induced emission property: synthesis, mechanofluorochromism, and mercury(II) detection. ACS Appl Mater Interfaces 2019;11:34232-40.
[16] Mulay SV, Dishi O, Fang Y, Niazi MR, Shimon LJW, Perepichka DF, Gidron O. A macrocyclic oligofuran: synthesis, solid state structure and electronic properties. Chem Sci 2019;10:8527-32 .
[17] Gopalakrishna TY, Zeng W, Lua X, Wu J. From open-shell singlet diradicaloids to polyradicaloids. Chem Commun 2018;54:2186-99.
[18] Leroyer L, Lepetit C, Rives A, Maraval V, Saffon-Merceron N, Kandaskalov D, Kieffer D, Chauvin R. From hexaoxy-[6]pericyclynes to *carbo*-cyclohexadienes, *carbo*-benzenes, and dihydro-*carbo*-benzenes: synthesis, structure, and chromophoric and redox properties. Chem Eur J 2012;18:3226-40.
[19] Chauvin R. "Carbomers". I. A general concept of expanded molecules. Tetrahedron Lett 1995;36 (3):397-401.
[20] a) Maraval V, Chauvin R. From macrocyclic oligo-acetylenes to aromatic ring *carbo*-mers. Chem Rev 2006;106:5317-43; b) Zou C, Lepetit C, Coppel Y, Chauvin R. Ring *carbo*-mers: from questionable homo-aromaticity to bench aromaticity. Pure Appl. Chem.

2006;78:791-811; c) Cocq K, Lepetit C, Maraval V, Chauvin R. "*Carbo*-aromaticity" and novel *carbo*-aromatic compounds. Chem Soc Rev 2015; 44:6535-59; d) Cocq K, Barthes C, Rives A, Maraval V, Chauvin R. Synthesis of functional *carbo*-benzenes with functional properties: the C2 tether key. Synlett 2019;30:30-43.
[21] a) Godard C, Lepetit C, Chauvin R. DFT exploration of structural and magnetic properties of [n]annulene ring carbomers. Chem Commun 2000;1833-4; b) Lepetit C, Godard C, Chauvin R. Aromaticity and homoaromaticity of annulene ring carbomers. New J Chem 2001;25:572-80; c) Lepetit C, Silvi B, Chauvin R. ELF analysis of out-of-plane aromaticity and in-plane homoaromaticity in carbo[N]annumenes and [N]pericyclynes. J Phys Chem A 2003;107:464-73; d) Chauvin R, Lepetit C, Maraval V, Leroyer L. Variation of aromaticity by twisting or expanding the ring content. Pure Appl Chem 2010;82(4):769-800; e) Cocq K, Maraval V, Saffon-Merceron N, Chauvin R. *Carbo*-benzene's aromaticity, before and beyond: a tribute to Nozoe. Chem Records 2015;15:347-61.
[22] Cocq K, Maraval V, Saffon-Merceron N, Saquet A, Poidevin C, Lepetit C, Chauvin R. *Carbo*-quinoids: stability and reversible pro-aromatic character towards *carbo*-benzenes. Angew Chem Int Ed 2015;54:2703-6.
[23] Li Z, Smeu M, Rives A, Maraval V, Chauvin R, Ratner MA, Borguet E. Towards graphyne molecular electronics. Nat Commun 2015;6:6321.
[24] Zhu , Wang TH, Su CJ, Lee SL, Rives A, Duhayon C, Kauffmann B, Maraval V, Chen Ch, Hsu HF, Chauvin R. 3D and 2D supramolecular assemblies and thermotropic behavior of a *carbo*-benzenic mesogen. Chem Commun 2017;53:5902-5.
[25] a) Rives A, Baglai I, Malytskyi V, Maraval V, Saffon-Merceron N, Voitenko ZV, Chauvin R. Highly π electron-rich macro-aromatics: bis(p-aminophenyl)-*carbo*-benzenes and their DBA acyclic references. Chem Commun 2012:48;8763-5; b) Listunov D, Duhayon C, Poater A, Mazères S, Saquet A, Maraval V, Chauvin R. Steric/π-electronic insulation of the *carbo*-benzene ring: dramatic effect of tert-butyl vs phenyl crowns on geometric, chromophoric, redox and magnetic properties. Chem Eur J 2018;24:10699-710; c) Baglai I, Maraval V, Bijani C, Saffon-Merceron N, Voitenko Z, Volovenko YM, Chauvin R. Enhanced π-frustration in *carbo*-benzenic chromophores. Chem Commun 2013:49;8374-6.
[26] Baglai I, De Anda-Villa M, Barba-Barba RM, Poidevin C, Ramos-Ortíz G, Maraval V, Lepetit C, Saffon-Merceron N, Maldonado JL, and Chauvin R. Difluorenyl *carbo*-benzenes: synthesis, electronic structure, and two-photon absorption properties of hydrocarbon quadrupolar chromophores. Chem Eur J 2015;21:14186-95.
[27] a) Leroyer L, Zou C, Maraval V, Chauvin R. Synthesis and stereochemical resolution of a [6]pericyclynedione: Versatile access to pericyclynediol precursors of *carbo*-benzenes. C R Chimie 2009;12:412-29; for early references on pericyclynes, see: b) Scott LT, DeCicco GJ, Hyun JL, Reinhardt G. Decamethyl[5]pericyclyne. A novel homoconjugated cyclic polyacetylene. J Am Chem Soc 1983;105:7760-1; c) Scott LT, DeCicco GJ, Hyun JL, Reinhardt G. Pericyclynes of order [5], [6], [7] and [8]. Simple convergent syntheses and chemical reactions of the first homoconjugated cyclic polyacetylenes. J Am Chem Soc 1985;107:6546-55.
[28] Ringenbach C, De Nicola A, Ziessel R. A concise modular synthesis of 2,5-diethynyl-3,4-dibutyl-thiophene-bridged back-to-back terpyridine ligands. J Org Chem 2003;68:4708-19.

[29] Corey EJ, Fuchs PL. A synthetic method for formyl → ethynyl conversion (RCHO → RC≡CH or RC≡CR). Tetrahedron Lett 1972;36:3769-72.
[30] Crystal data for **2a**. Formula: $C_{86}H_{90}S_2$, M = 1187.70, Triclinic, a = 9.6897(2) Å, b = 11.3553(2) Å, c = 17.4435(4) Å, α = 101.9684(18)°, β = 99.1771(18)°, γ= 109.0421(19)°, V = 1720.48(4) Å^3, T = 130 K, space group P-1, Z = 1, μ(Cu-Kα) = 1.031 mm^{-1}, 22189 reflections measured, 6693 unique (Rint = 0.0172), 6055 reflections used in the calculations [I > 3σ(I)], 397 parameters, R1 = 0.0355, wR = 0.0486. CCDC 2027203 contains the supplementary crystallographic data for **2a**. These data can be obtained free of charge from The Cambridge Crystallographic Data Centre via http://www.ccdc.cam.ac.uk/data_request.cif.
[31] Zhu C, Rives A, Duhayon C, Maraval V, Chauvin R. Lipidic *carbo*-benzenes: molecular probes of magnetic anisotropy and stacking properties of α-graphyne. J Org Chem 2017;82:925-35.
[32] Phulwale BV, Mishra SK, Nec M, Mazal C. Phenanthrylene-butadiynylene and phenanthrylene-thienylene macrocycles: synthesis, structure, and properties. J Org Chem 2016;81:6244-52.
[33] Yousaf M, Zarate X, Schott E, Lough AJ, Koivisto BD. Photophysical behavior of BODIPY-phenylacetylene macrocyclic dyads for light-harvesting applications. RSC Adv 2018;8:28533-7.
[34] Phulwale BV, Mishra SKMazal C. Synthesis and properties of π-conjugated donor-acceptor macrocycles derived from phenanthrylene building blocks. Tetrahedron 2018;74:3616-23.
[35] Zhao YL, Liu Q, Zhang JP, Liu ZQ. Heteroatom-substituted expanded radialenes: one-pot synthesis and characterization of expanded 1,3-dithiolane[n]radialenes. J Org Chem 2005;70:6913-7.
[36] Fang Z, Samoc M, Webster RD, Samoc A, Lai YH. Triphenylamine derivatized phenylacetylene macrocycle with large two-photon absorption cross-section. Tetrahedron Lett 2012;53:4885-8.
[37] Bhaskar A, Guda R, Haley MM, Goodson III T. Building symmetric two-dimensional two-photon materials. J Am Chem Soc 2006;128:13972-3.
[38] Li T, Zhang D, Wang R, Fan Y, Guo X, Liu S, Ma Y, Zhao D. Synthesis, solvent-dependant emission and two-photon absorption of a triangular –[D-π-A]3- macrocycle. Org Chem Front 2017;4:737-42.
[39] Pyun OS, Yang W, Jeong MY, Lee SH, Kang KM. Synthesis and two-photon absorption property of phenylacetylene macrocycles. Tetrahedron Lett 2003;44:5179-82.
[40] Nakao K, Nishimura M, Tamachi T, Kuwatani Y,
Miyasaka H, Nishinaga T, Iyoda M. Giant macrocycles composed of thiophene, acetylene, and ethylene building blocks. J Am Chem Soc 2006;128:16740-7.
[41] Kim KS, Noh SB, Katsuda T, Ito S, Osuka A, Kim D. Charge transfer induced enhancement of near-IR two-photon absorption of 5,15-bis(azulenylethynyl)zinc(II) porphyrins. Chem Commun 2007;2479-81.
[42] Sheng N, Gu B, Ren B, Zhang J, Wang Y, Sha J. A series of polycyclic aromatic hydrocarbon-substituted metal-free porphyrins: substituent effect on two-photon absorption property. Dyes and Pigments 2017;142:116-20.

[43] Yoon ZS, Cho DG, Kim KS, Sessler JL, Kim D. Nonlinear optical properties as a guide to aromaticity in congeneric pentapyrrolic expanded porphyrins: pentaphyrin, sapphyrin, isosmaragdyrin, and orangarin. J Am Chem Soc 2008;130:6930-1.
[44] a) Lim JM, Yoon ZS, Shin JY, Kim KS, Yoon MC, Kim D, The photophysical properties of expanded porphyrins: relationships between aromaticity, molecular geometry and non-linear optical properties Chem. Commun., 2009; 261–73; b) Yoon ZS, Kwon JH, Yoon MC, Koh MK, Noh SB, Sessler JL, Lee JT, Seidel D, Aguilar A, Shimizu S, Suzuki M, Osuka A, Kim D. Nonliear optical properties and excited-state dynamics of highly symmetric expanded porphyrins. J Am Chem Soc 2006;128:14128-34.
[45] Gouterman M. Spectra of porphyrins. J Mol Spectrosc 1961;6:138-63.
[46] Demchenko AP, Tomin VI, Chou PT. Breaking the Kasha Rule for more efficient photochemistry. Chem Rev 2017;117:13353-81.
[47] Itoh T. Fluorescence and phosphorescence from higher excited states of organic molecules. Chem Rev 2012;112:4541-68.
[48] Wild UP, Griesser HJ, Tuan VD, OTH JFM, Fluorescence from the second excited singlet state of [18] annulenes. Chem. Phys. Lett. 1976;41:450-55.
[49] a) Lukaszewicz A, Karolczak J, Ziolek M, Kowalska D, Maciejewski A, Steer RP. Photophysical processes in electronic states of zinc tetraphenyl porphyrin accessed on one- and two-photon excitation in the soret region. Chem Phys 2007;331:359-72; b) Yu HZ, Baskin JS, Zewail AH. Ultrafast dynamics of porphyrins in the condensed phase: II. Zinc tetraphenylporphyrin. J Phys Chem A 2002;106:9845-54.
[50] Mena-Osteritz E, Zhang F, Götz G, Reineker P, Bäuerle P. Optical properties of fully conjugated cyclo[n]thiophenes – an experimental and theoretical approach. Beilstein J Nanotechnol 2011;2:720-6.
[51] Principles and Applications of Quantum Chemistry, V.P. Gupta, Academic Press (2016).
[52] Esipova TV, Rivera-Jacquez EJ, Weber B, Masunov AE, Vinogradov SA. Two-photon absorbing phosphorescent metalloporphyrins: effects of π-extension and peripheral substitution. J Am Chem Soc 2016;138:15648-62.
[53] a) Palatinus L, Chapuis G, *J. Appl. Cryst.*, 2007, **40**, 786-790; b) Betteridge P W, Carruthers J R, Cooper R I, Prout K, Watkin D J, *J. Appl. Cryst.*, 2003, **36**, 1487; c) International Tables for X-ray Crystallography, vol. IV, Kynoch Press, Birmingham, England, 1974.
[54] Van De Wetering K, Brochon C, Ngov C, Hadziioannou G. Design and synthesis of a low band gap conjugated macroinitiator: toward rod-coil donor-acceptor block copolymer. Macromolecules 2006;39:4289-97
[55] Guo K, Hao J, Zhang T, Zu F, Zhai J, Qiu L, Zhen Z, Liu X, Shen Y. The synthesis and properties of novel diazo chromophores based on thiophene conjugating spacers and tricyanofuran acceptors. Dyes and Pigments 2008;77:657-64.
[56] Koeckelberghs G, De Groof L, Pérez-Moreno J, Asselberghs I, Clays K, Verbiest T, Samyn C. Synthesis and nonlinear optical properties of linear and Λ-shaped pyranone-based chromophores. Tetrahedron 2008;64:3772-81.
[57] a) Sheik-Bahae M, Said AA, Wei TH, Hagan DJ, Van Stryland EW. Sensitive measurement of optical nonlinearities using a single beam. IEEE J Quantum Electron 1990;26(4):760-9; b) Stryland EWV, Sheik-Bahae M. Z-Scan Measurements of Optical Nonlinearities (1998).
[58] Ganeev RA, Ryasnyansky AI, Baba M, Suzuki M, Ishizawa N, Turu M, Sakakibara S, Kuroda H. Nonlinear refraction in CS2. Appl Phys B 2004;78(3–4):433-8.

[59] Chen CH, McCann MP. Measurements of two-photon absorption cross sections of common blue dyes. Opt Commun 1987;63(5):335-8.

Graphical abstract